Paleolatitudes of the Permo-Triassic Ukrainian Shield with Implications for Pangaea A and B

Kenneth Yuan[1], Van der Voo, R.[2*], Bazhenov, M.[3], Bakhmutov, V.[4], Alekhin, V.[5], Hendriks, B.W.H.[6]

[1] *Department of Geological Sciences, University of Michigan, Ann Arbor, MI,48109-1005, USA, kenyuan@umich.edu*

[2*] *Corresponding Author: Department of Geological Sciences, University of Michigan, Ann Arbor, MI,48109-1005, USA, voo@umich.edu, Telephone: +1-734-7648322, fax: +1-734-7634690*

[3] *Geological Institute of the Russian Academy of Sciences, Moscow, Russia, mibazh@mail.ru*

[4] *Geophysics of the National Academy of Science of Ukraine, Kiev, Ukraine, bakhmutovvg@gmail.com*

[5] *Donetsk Technical University, Donetsk, Ukraine, vikalex07@rambler.ru*

[6] *Geological Survey of Norway, Trondheim, Norway, Bart.Hendriks@ngu.no*

Abstract

Three research teams jointly collected and independently analyzed 306 samples from Permian and Triassic dikes from the Ukrainian Shield, the southwest portion of the East European Craton. This paper presents well-documented paleomagnetic results from samples that are not affected by inclination shallowing, are from a tectonically stable region (Alexandre et al., 2004), and have good age dates. The results are: andesites, Dec/Inc = 240.1° / -64.4°, k = 96, alpha-95 = 4.5, N = 12; trachytes, Dec/Inc = 205.6° / -21.4°, k = 23 alpha-95 = 7.0, N = 20. Argon-argon dating places the andesites in the upper Late Triassic at 202.6-216.9 Ma and the trachytes in the early Artinskian (mid-Early Permian) at 282.6 ± 2.6 Ma. These are the first paleomagnetic results from these dikes that are based on a fully demagnetized large collection with good age control. The paleolatitude of andesite emplacement is 46.2°N.

The paleolatitude of the trachytes is 11.1°N. With Gondwana in the paleoposition used by Muttoni et al. (2003) for about 280 Ma, this paleolatitude of Baltica neither allows Pangaea A, nor disproves Pangaea B. However, if the Gondwana paleoposition is changed to a paleopole at 30°S, 54.9°E (Torsvik and Van der Voo, 2002), then Pangaea A-type reconstructions become possible. A more reliable mid-Early Permian paleopole for cratonic Gondwana would provide a more definitive conclusion.

Keywords: Paleomagnetism; Pangaea: Ukrainian Shield; Permo-Triassic; Baltica

1. Introduction

Paleomagnetic data collected from the Permian and Triassic imply an impossible overlap between Gondwana and Laurasia by eleven degrees of latitude (Muttoni et al., 2003) when the continents are longitudinally constrained as in conventional Pangaea reconstructions. To solve this conundrum an alternate reconstruction called Pangaea B (Figure 1) has been proposed that places Gondwana and Laurussia in non-competing areas (Bachtadse et al., 2002; Muttoni et al., 2009). Pangaea A, the configuration proposed by Alfred Wegener, refined by Bullard et al (1965), and often cited in textbooks, juxtaposes the northwestern coast of Africa and the Appalachian mountain belt in North America. In Pangaea B, Western Europe is located to the north of the north coast of South America instead (Crasquin-Soleau et al., 2001). The Atlantic Ocean opened in the Jurassic (Schettino and Turco, 2009) and all agree that by that time Western Europe was longitudinally connected to the north coast of Africa. To arrive at a Pangaea-A type fit in the Early Jurassic, a dextral mega-shear of some 3500 km is necessary between Gondwana and Laurussia, for which little geological evidence exists (Torsvik and Cocks, 2004).

The eleven degree overlap could have been caused by inclination shallowing in sedimentary rocks. Therefore, collecting igneous rocks unaffected by inclination shallowing could help solve this problem (Rochette and Vandamme, 2004). Non-dipole fields and other geomagnetic field complexities have also been proffered (Van Der Voo and Torsvik, 2001; Vizán and Zele, 2007), but this paper proposes the application of Occam's razor, i.e., identifying the simplest solution as usually being correct, in the expectation that higher quality paleomagnetic results collected from critical areas will substantiate the original scheme of Pangaea A's reconstruction (Van der Voo and Torsvik, 2004) and will render the Pangea-B model unnecessary.

306 Permian and Triassic dike samples were collected from 43 dikes and a couple of their baked-contact rocks from the Ukrainian Shield in the East European Craton (Fig. 2; Gee, 2004). This area forms part of the Baltica proto-plate (Mikhailova and Kravchenko, 1986) and is an

ideal place to sample for paleomagnetic studies because it has been a relatively tectonically stable area since the Early Permian.

2. Geology and Sampling

The East European Craton (EEC) formed 1.8-1.7 billion years ago when Fennoscandia, Sarmatia and Volga-Uralia amalgamated. The craton has never been torn completely apart but has undergone several tectonic processes, such as extension and rifting starting as early as 1.65 Ga. The EEC was later incorporated as Baltica into Rodinia 1.2-0.9 billion years ago (Bogdanova et al., 2008) and after the breakup of Rodinia, and independent drift during the earlier Paleozoic, it became part of Laurussia and then Pangaea.

Sarmatia can be divided into the Voronezh Massif in the north and the Ukrainian Shield in the south (Glasmacher et al., 2004). The Voronezh massif and the Ukrainian shield have been joined together since the Achaean (Shchipansky and Bogdanova, 1996). From the Carboniferous to Permian Period, there were compressional events and earlier-formed basins inverted. During the Permo-Triassic, there was weak rifting in those basins, which resulted in basaltic magmatism (Nikishin et al., 1996).

43 trachytic and andesitic sites, where each site is assumed to be a separate cooling unit, were drilled all along the eastern side of the Ukrainian shield. The collection was divided into three batches and these were measured by the different groups of researchers from the U.S., Russia and Ukraine.

3. Mineralogy

A scanning electron microscope (SEM) from the University of Michigan Electron Microbeam Analysis Laboratory was used to verify the presence of iron oxides whose unblocking temperatures were revealed by thermal demagnetization. Three representative samples were examined: one andesite sample whose main magnetic carrier is (titano-)magnetite (Fig. 3); one andesite sample whose main carriers are (titano-)magnetite and hematite (Fig. 4); and one trachyte sample whose main carriers are hematite (Fig. 5). Interestingly, the andesites contained Fe-oxides with up to 42 percent titanium. The effects of the titanium content and the contributions of the grains observed with the SEM to the paleomagnetism of the samples are most likely not important, because (1) the Ti-content is rather high and (2) these grains are too large (greater than 20 μm) to be stably magnetized as single- or pseudo-single domain grains. The high titanium content would lower the unblocking temperatures (Fig. 6) and indeed we see a little of that in the thermal demagnetization plots, but not to any significant extent.

However, we can deduce from the rather fresh appearance of the Fe-oxides in the andesites as well as the trachytes that hydrothermal alteration of the samples has not been severe and that evidence for oxidation to maghemite (e.g., shrinkage cracks) is not readily observed.

4. Paleomagnetic and Age Dating Methodologies

In the laboratory the cylindrical field-drilled paleomagnetic samples were sawed to two specimens with 2.2 cm height. The specimens were labeled “A” for the innermost portion of the samples and “B” for the outermost portion nearest the rock’s originally exposed surface. The samples were then cleaned with a damp towel and dried. Afterwards, a sample’s orientation line and its number were painted with non-magnetic, white, heat-resistant glaze. Samples that cracked during any of the preparations were molded back together with non-magnetic alumina cement.

The samples studied at the University of Michigan were stored and treated inside the magnetically shielded room of its paleomagnetic laboratory, to minimize the acquisition of viscous magnetization overprinting. The natural remnant magnetization (NRM) of the samples was measured using a three-axis 2G magnetometer. The specimens were thermally demagnetized in an ASC TD-48 oven in the shielded room where the residual field did not exceed 200 nT.

Measurements were processed with a Labview module called MichCryo7 that plots the data as vector endpoints (Zijderveld, 1967) and in stereonets. The magnetization directions were calculated using the computer program Super-IAPD (Torsvik, 2000), which uses principal component analysis (Kirschvink, 1980). Vectorial trajectories were analyzed, except in cases where endpoints plotted along great circle paths, in which case the software program PaleoMac (Cogné, 2009), which includes stable-endpoint observations (McFadden and McElhinny, 1988), was used. After characteristic directions and site means were obtained with Super IAPD and Fisher (1953) statistics, paleopoles were calculated with Paleomac.

age dating and mineral separation used standard techniques. Before packing in Al-foil, mineral separates were hand-picked under a binocular microscope and all samples were rinsed in alternating acetone and distilled water. The sample packets were stacked and loaded in a sealed Al-capsule with Cd-shielding for irradiation in the 5C site at the McMaster Nuclear Reactor facility, Hamilton, Canada. The samples were irradiated at McMaster for 16h40m at 3 MW (50 MWH) with nominal neutron flux of 4 x 10e13 —— ; nominal temperature in the irradiation site is <50°C (M. Butler, pers. comm.). Production of isotopes from Ca and K were determined by irradiation of CaF and K2SO4 salts; values of —— = 0.000169, —— =

0.000736, and —— = 0.032593 were used. Neutron fluence was monitored with Tinto biotite of 410.3 Ma (Rex and Guise, 1995). We incorporated a conservative 1% error in J-value for all unknowns.

Samples were analyzed in the $^{40}Ar/^{39}Ar$ Geochronology Laboratory of the Norwegian Geological Survey (NGU). Gas from irradiated samples was released in a step-wise fashion from a resistance furnace. Furnace conditions are similar to those described in Eide et al. (2002). Gas released from a sample at a single temperature step was cleaned in the extraction line for 11 minutes using two pairs of SAES AP-10 getters, mounted in isolated sections of the line, each maintained with their own vacuum pumps. The purified gas was then analyzed on a MAP 215-50 mass spectrometer. Data for blanks, monitors and unknowns were collected on a Johnson electron multiplier with gain setting at 1, while the magnet was automatically scanned over masses 35 through 41 in a cycled, 'peak-hop' mode. Masses 37 through 40 were each measured in ten cycles and 10 counts per mass per cycle; mass 36 was measured with 20 counts per cycle.

Dynamic blank measurements on mass 40 indicate a stable background (1.0×10^{-13} ccSTP). Background levels (blanks) for the furnace were measured at 100 to 200°C temperature increments prior to each sample analysis. Furnace blanks were maintained at levels of < 1.1×10^{-11} ccSTP for mass 40 and 3 - 5×10^{-14} ccSTP for mass 36 at temperatures of 500 through 1000°C; blanks increased to 3.0×10^{-11} ccSTP for mass 40 and 1.1×10^{-13} ccSTP for mass 36 at high temperatures (1200-1400°C). Background levels of masses 37 and 39 did not change signficantly from dynamic blank levels at any temperature (1×10^{-13} ccSTP for mass 37; <5.3×10^{-14} ccSTP for mass 39). Background levels for mass 38 were < 3×10^{-14} ccSTP at all temperatures. At experimental temperatures between 600 and 1000°C, furnace blanks for mass 40 typically were <1% of the sample signal size.

Data from unknowns were corrected for blanks prior to being reduced with the IAAA (Interactive Ar-Ar Analysis) software package (Visual Basic programming for PC Windows) written by T.H. Torsvik and N.O. Arnaud and based in part on equations in Dalrymple et al. (1981) and McDougall & Harrison (1999). Data reduction in IAAA incorporates corrections for interfering isotopes, mass discrimination (measured with an air pipette), error in blanks and decay of .

5. Age Dating Results

Eight andesite and one trachyte sample yielded hornblende crystals irradiated for age dating. Of the eight andesite samples, five gave meaningful results; these results are summarized in Table 3. The dating places the andesites in the Late Triassic at 202.6-216.9 Ma. One characteristic andesite age spectrum (sample M1234), which corresponds to site K111-K117, is shown in Figure 7 and its isochron is shown in Figure 8.

Notice that the three steps at about 209 Ma in Figure 7 represent 79% of the argon released and that they form an accurate and unambiguous plateau. The other four andesite sample ages all have similarly good behavior; they all fall within ten million years of 209 Ma and thus help verify that the andesites are Late Triassic in age.

On the other hand there was only one trachyte sample (from site M1171) that yielded a suitable potassic mineral for age dating. Its age spectrum is shown in Figure 9 and its K/Ca ratio is shown in Figure 10. The age of 282.6 ± 2.6Ma indicates that the trachytes are mid-Early Permian (Artinskian) in age.

The ages, along with the paleopoles calculated from the results of the andesites and trachytes (to be discussed next), can be used to refine the Eurasian APWP and indicate that the continent moved significantly northward in the Early Permian to Late Triassic interval, which is what was expected.

6. Andesites: Paleomagnetic Results

The andesites were collected from blocky, solid, and relatively unaltered dikes, thus making them suitable for paleomagnetism. Thermal demagnetization showed that most of the samples had no overprint magnetizations that may have been introduced by alteration or growth of viscous remanence. A typical example of a thermal demagnetization of an andesite sample with a nearly univectorial decay is shown in Figure 11 and reveals the characteristic steeply up and southwesterly direction of this suite of dikes.

On close inspection, however, it can be seen from the remanence-versus-temperature plots (e.g., Fig. 11) that there are actually two magnetic minerals that carry such characteristic directions. One component unblocks just below about 580°C at which point about 60% of the remanence is lost, and the other component unblocks below about 675°C (Fig. 11). Both components have the same characteristic SW and steeply up, or NE and steeply down magnetization (Figs. 11, 12) and they cannot be distinguished from each other. The unblocking temperatures indicate that magnetite and hematite are the most likely carriers of these two components. Site-mean directions of the SW/up and NE/down directions are shown in Figures 13 and 14 and they are interpreted as representing reversed and normal polarity magnetizations. Where magnetite and hematite both carry the characteristic remanence, not only are their directions the same, but also their polarity; thus, we have no reason to think that the magnetite and hematite magnetizations are of different age. A reversal test on the directions of all the sites (N=12) passes McFadden and McElhinny's reversal test (1990) with a B level type classification.

Three of the 15 dikes (and their bakes contacts) have either aberrant mean directions, statistical parameters that indicate poor clustering (e.g, α_{95} >20), or no measurable remanence above treatments at ~ 200°C.

The andesite site K 111-117 intruded into Devonian basalts, where samples K 104 – 110 were heated by the intrusion. The baked basalt samples have directions that are statistically identical to those of the intruding andesite dike (Table 1). In contrast, basalt samples farther away as well as a trachyte dike located 5 m away from the andesite dike have a different direction of magnetization; these are represented in Table 1 as sites K 097-103 and K 094-096. The magnetizations of these sites will be briefly discussed in the next section. Suffice for now to mention our conclusion that the baked contact test of sites K111-117 and K104-110, plus the recognition that host rocks farther away from the andesite dike have not been reset, constitute a fully positive contact test.

As mentioned, ^{40}Ar-^{39}Ar dating of five samples places the andesites at 209.7 ± 7.1 Ma (202.6-216.9 Ma), representing the Late Triassic magnetic field with an overall mean andesite dike direction of Dec/Inc = 240.1 degrees / -64.4 degrees, k = 96, alpha-95 = 4.5, N = 12, which indicates a paleolatitude of 46.2°N and a VGP at 50°N, 106.4°E, dp=5.8, dm=7.2 (Fig. 15).

7. Trachytes: Paleomagnetic Results

The trachytes have an aphanitic texture and were not as easily drilled as the andesites because the former were more friable. Although the samples came from large blocky rock outcrops, the trachytes were generally more weathered (confirmed later in the demagnetization characteristics by relatively large overprints). This may well be because the trachytes are significantly older than the andesites and may have had a more complex history. The trachytes formed some seventy million years earlier at around 280-285 Ma and may have suffered somewhat from the last phases of deformation in the nearby Dniepr-Donets aulacogen and Donbass fold belt, which started rifting in the Devonian and had periods of extension and deformation throughout the Late Carboniferous into the Early Permian (Vai, 2003; Saintot et al. 2003; Kostyuchenko et al. 2008). The extension, later compressional inversions, and reheating of the area, could have affected the magnetization and quality of the trachyte samples, but not the younger andesites.

The trachyte site K 097 – 103 intruded into the same Devonian basalts, with samples K094-096, as were collected for a baked contact test with an andesite dike. The directions of the three samples K 094-096 are very similar to those of the trachyte and appear to reflect a resetting by the intruding dike. This constitutes a contact test, which is partial-positive because we have no information on the direction of the country rock away from the intrusion.

The trachytes have characteristic directions that are shallowly up and south-southwest (100% reversed polarity) as can be seen in Figure 16. The site with samples K97-K103 is representative of the trachyte characteristics. The remanence contributors are hematite and magnetite (Fig. 17, 18) , which, importantly, both reveal the same direction. The mean direction (Tables 1, 2; Figure 18) of 20 (out of 27) trachyte dikes is Dec/Inc = 205.6° / -21.4°, k = 23.0, alpha-95 = 7.0, N = 20. Excluded from the mean are sites with poor statistical parameters, lack of characteristic remanence above ~200°C, or highly aberrant directions, as explained in the footnotes of Table 1.

One of the andesite dikes (K111-K117) intruded into a Devonian basalt, K104-K110, and one of the trachyte dikes, K097-K103, intruded into a very nearby Devonian basalt K094-K096.

The basalts were only five meters apart from each other and it is inferred that the K094-K096 and K104-K110 come from the same Devonian basalt. The K094-K096 has been affected by the trachyte intrusion of K097-K103 because the K094 and K095 point very shallowly up and Artinskian directions while the K096 points close to Artinskian directions. Samples K104-K110 have been completely reset by the nearby andesite intrusion of K111-117 and share the similar directions. Therefore, we believe that the magnetization of the trachytes is primary based on a positive partial baked contact test.

Argon-argon dating of one sample places the trachytes at 280-285.2 Ma (Figure 9). Six steps in the argon release spectrum are chronologically very close to each other and differ by less than ten million years. Thus the mid-Early Permian geomagnetic field is interpreted to have a direction of Dec/Inc = 205.6° / -21.4°, k = 23.0, alpha-95 = 7.0, N = 20, which suggests a paleolatitude of 11.1° for the Ukrainian sampling area and a VGP at 47.5° N, 179.2° E, dp=3.9, dm=7.4.

8. Discussion

The site-mean directions of the andesite and trachyte dikes have been combined into overall mean directions (Table 2), from which paleopoles have been computed (using Paleomac; Cogné, 2009). Our new poles were compared to those of the apparent polar wander path (APWP) of Baltica (Figure 19; Torsvik et al., 2008).

We argue that these new paleopoles are reliable representations of the geomagnetic field at the time these dikes cooled upon intrusion. The sampling area is thought to have been tectonically stable since the Early Permian, there is no indication of inclination error or significant anisotropy of the dike material, there is a positive reversal test and a positive partial contact test for the Late Triassic and the mid-Early Permian respectively, and the demagnetization trajectories give no indication of contamination by partially overlapping overprint components. The magnetic carriers are magnetite and hematite, which could indicate post-intrusion oxidation, but the directions of the magnetizations carried by these minerals are invariably the same within measurement error.

The corresponding paleolatitudes at 11.1°N for the trachytes and 46.2°N for the andesites mean that Ukraine moved from a southerly, near-equatorial latitude in the Early Permian to a much more northerly latitude by the Late Triassic. Permian fossils verify that Ukraine was in a warm, equatorial climate at that time (White 1904).

In terms of the paleomagnetic implications from these new results, they allow more latitudinal room for a mid-Early Permian Pangaea A type fit because the trachyte result places Baltica in a somewhat more northerly position than previous poles indicated. A recent study of Early Permian (Asselian, ~293Ma) sedimentary strata in the Donbas Foldbelt determined a paleolatitude of 16°N (Meijers et al., 2010). If these sedimentary rocks suffered some inclination shallowing, this paleolatitude would possible be on the low side and a correction for the shallowing would increase the paleolatitude.

Our Permian results satisfy four Q criteria while the Triassic satisfy six. The Permian rocks have well determined rock ages, a sufficient number of samples, adequate demagnetization and no resemblance to later paleopoles. They pass a partial baked contact test, which does not contribute to Q, and have inferred but not proven structural control. Thirdly, there are generally no normal-polarities observed in Early Permian strata, and our rocks are no exception. On the other hand, our results are unlikely to have suffered from inclination shallowing. To be on the conservative side, we claim a Q = 4 for our 282 Ma (mid-Early Permian) rocks.

The Triassic rocks satisfy six Q criteria, they have well determined rock ages, a sufficient number of samples, adequate demagnetization, one or more magnetic reversals, a positive contact test, and no resemblance to later paleopoles. Not satisfying the Q criteria are considerations of complete structural control. The Late Triassic results are not affected by inclination shallowing.

9. Conclusions

New paleomagnetic results show that Ukraine was at 11.1°N and possibly as northerly as 18°N (Meijers et al., 2010). With Gondwana in the paleoposition used by Muttoni et al. (2003) for about 280 Ma, the paleolatitude of 11.1°N of Baltica neither allows Pangaea A, nor disproves Pangaea B. However, with the slightly higher paleolatitude for Baltica than that used by Muttoni and colleagues (~9°N for Ukraine), and using the Gondwana paleopole at 30°S, 54.9°E from Torsvik and Van der Voo (2002), then Pangaea A-type reconstructions become possible, because the latter Gondwana pole allows more room for a Pangaea A type fit, as shown in Figure 20.

Although contributions from an octupole field cannot be ruled out, we now prefer to favor the idea that more reliable paleomagnetic directions can solve the Pangaea problem in the near future. Clearly, a more reliable mid-Early Permian paleopole for cratonic Gondwana would be desirable.

Acknowledgements

The authors would like to express their gratitude to Evgeny Polyashenko for his help in the field. He helped collect many of the samples and provided invaluable fieldwork experience to the team. The authors would also like to thank the Geological Sciences Department of the

National Taras Shevchenko University of Kyiv for their role in transporting the samples. Finally, the support from the National Science Foundation grant EAR-0634807 made this project possible and is very gratefully appreciated.

REFERENCES

Alexandre, P., F. Chalot-Prat, A. Saintot, J. Wijbrans, R. Stephenson, M. Wilson, A. Kitchka, and S. Stovba. The $^{40}Ar/^{39}Ar$ dating of magmatic activity in the Donbas Fold Belt and the Scythian Platform (Eastern European Craton). Tectonics 23 (2004): 1-15.

Bachtadse, Valerian, Rainer Zanglein, Jennifer Tait, and Heinrich C. Soffel. Paleomagnetism of the Permo-Carboniferous (280 Ma) Jebel Nehoud ring complex, Kordofan, Central Sudan. Jour. Afr. Earth Sci. 35 (2002): 89-97.

Bogdanova, S. V. The East European Craton: Some Aspects of the Proterozoic Evolution in its South-west, Polskie Towarzystwo Mineralogiczne - Prace Specjalne (Mineralogical Society of Poland – Special Papers) 26 (2005): 18–24.

Bogdanova, S. V., B. Bingen, R. Gorbatschev, T. N. Kheraskova, V. I. Kozlov, V. N. Puchkov, and Yu. A. Volozh. The East European Craton (Baltica) before and during the assembly of Rodinia. Precambrian Res. 160 (2008): 23-45.

Bullard, E.C., J. E. Everett, A. G. Smith. A symposium on continental drift IV. The fit of the continents around the Atlantic. Phil. Trans. Roy. Soc. London, Ser. A: v.258 (1965): 41-51.

Cogné, J. P. Paleomac. Université de Paris. Web. April & May 2009. <http://www.ipgp.fr/~cogne/pub/paleomac/PMhome.html>.

Crasquin-Soleau, S., J. Broutin, J. Besse, and M. Berthelin. Ostracods and paleobotany from the middle Permian of Oman: implications on Pangaea reconstruction. Terra Nova 13 (2001): 38-43.

Dalrymple, G.B., E.C. Alexander, M.A. Lanphere and G.P. Kraker. Irradiation of samples for $^{40}Ar/^{39}Ar$ dating using the Geological Survey TRIGA reactor. Geol. Surv. Professional Paper 1176 (1981): 1-55.

Danišík, M., R.F. Sachsenhofer, V.A. Privalov, E.P. Panova, W. Frisch, C. Spiegel. Low-temperature thermal evolution of the Azov Massif (Ukrainian Shield–Ukraine) — Implications for interpreting (U–Th)/He and fission track ages from cratons. Tectonophysics 456 (2008): 171-179.

Eide, E.A., P.T. Osmundsen, G.B. Meyer, M.A. Kendrick and F. Corfu, F. The Nesna Shear Zone, north-central Norway: An $^{40}Ar/^{39}Ar$ record of Early Devonian – Early Carboniferous ductile extension and unroofing. Norwegian Jour. Geol. 82 (2002): 317-339.

Fisher, R. A. Dispersion on a sphere. Proc. Royal Soc. A 217 (1953): 295-305.

Gee, D.G, and R.A Stephenson. The European lithosphere: an introduction. European Lithosphere Dynamics. Geol. Soc. Lond. Mem. 32 (2006): 1-9.

Glasmacher, U. A., W. Bauer, N. Clauer, and V. N. Puchkov. Neoproterozoic metamorphism and deformation at the southeastern margin of the East European Craton, Uralides, Russia. Intern. Jour. Earth Sci. 93 (2004): 921-44.

Irving, E. The Case for Pangea B, and the Intra-Pangean Megashear. In: Timescales of the paleomagnetic field, J.E.T. Channell, D.V. Kent, W. Lowrie and J. G. Meert, Editors, AGU Geophys. Monogr. 145 (2004): 13-27.

Ishikawa, Y., and S. Akimoto. Magnetic properties of the FeTiO,-Fe,O, solid solution series. Journ. of the Physical Society of Japan. 12 (1957): 1083-1098.

Jackson, Mike. MichCryo7. Computer Software. Vers. 1. Web.

Jeleńska, M., V. Bakhmutov and L. Konstantinienko. Paleomagnetic and rock magnetic data from the Silurian succession of the Dniester Basin, Ukraine. Phys. Earth Planet. Int. 149 (2005): 307-20.

Kirschvink, J.L. The least-squares line and plane and the analysis of palaeomagnetic data. Geophys. Jour. R. Astron. Soc., 62 (1980):699-718.

Kostyuchenko, S. L., A. F. Morozov, R. A. Stephenson, L. N. Solodilov, A. G. Vedrentsev, K. E. Popolitov, A. F. Aleshima, V. S. Vishnevskaya, and T. P. Yegorova. The evolution of the southern margin of the East European Craton based on seismic and potential field data. Tectonophysics 381 (2008): 101-118.

Livermore, R. A., A. G. Smith, and F. J. Vine. Late Paleozoic to early Mesozoic evolution of Pangaea. Nature 322 (1986): 162-65.

McDougall, I. and T.M. Harrison. Geochronology and Thermochronology by the ^{40}Ar/^{39}Ar method. Oxford Monographs on Geology and Geophysics no. 9, Second Edition. Oxford University Press, New York (1999): 269pp.

McFadden, P.L., and D.L. Jones. The fold test in paleomagnetism. Geophys. Jour. Roy. astr. Soc. 67 (1981): 53–58.

McFadden, P.L., and M.W. McElhinny. The combined analysis of remagnetization circles and direct observations in paleomagnetism. Earth Planet. Sci. Lett., 87 (1988): 161–172.

McFadden, P.L., and M.W. McElhinny. Classification of the reversal test in palaeomagnetism: Geophys. Jour. Intern. 103 (1990): 725–729.

Meijers, M, M.F. Hamers, D. van Hinsbergen, D. van der Meer, A. Kitchka, C. Langereis and R. Stephenson. New late Paleozoic paleopoles from the Donbas Foldbelt (Ukraine): implications for the Pangea A vs. B controversy, Earth Planet. Sci. Lett. (2010): in review

Mikhailova, N. P., and S. N. Kravchenko. The Late Proterozoic position of the Ukrainian Shield from paleomagnetic data. Jour. Geodyn. 7 (1986): 69-77.

Muttoni, G., D.V. Kent, E. Garzanti, P. Brack, N. Abrahamsen and M. Gaetani. Early Permian Pangaea 'B' to Late Permian Pangaea 'A' Earth Planet. Sci. Lett. 215 (2003): 379-94.

Muttoni, G., M. Gaetani, D.V. Kent, D. Scionnach, L. Angiolini, F. Berra, E. Garzanti, M. Mattei and A. Zanchi. Opening of the Neo-Tethys Ocean and the Pangea B to Pangea A transformation during the Permian. GeoArabia 14 (2009): 17-48.

Nikishin, A. M., A. V. Furne, and P. Ziegler. Riphaean-Vendian geologic history and geodynamics of the East-European Craton. Moscow University Geology Bulletin 52.4 (1997): 9-20.

Nikishin, A. M., P. A. Ziegler, R. A. Stephenson, S. A. Cloetingh, A. V. Furne, P. A. Fokin, E. V. Ershov, S. N. Bolotov, M. V. Korotaev, A. S. Alekseev, V. I. Gorbachev, E. V. Shipilov, A. Lankreijer, E. Yu. Bembinova, and I.V. V. Shalimov. Late Precambrian to Triassic history of the East European Craton: dynamics of sedimentary basin evolution. Tectonophysics 268 (1996): 23-63.

Pavlov, V. E., V. Courtillot, M. L. Bazhenov, and R. V. Veselovsky. Paleomagnetism of the Siberian Traps: New Data and a new overall 250 Ma pole for Siberia. Tectonophysics 443 (2007): 72-92.

Rex, D.C. and P.G.Guise. Evaluation of argon standards with special emphasis on time scale measurements. In Odin, G.S. (ed.) Phanerozoic Time Scale, 21-23. Bulletin Lias. Information, IUGS Subcommission on Geochronology 13 (1995).

Rochette, P., and D. Vandamme. Pangaea B: an artifact of incorrect paleomagnetic assumptions? Annali Geofis. 44 (2001): 649-58.

Saintot, A., R. Stephenson, S. Stovba and Yu. Maystrenko. Structures associated with inversion of the Donbas Foldbelt. Tectonophysics 373 (2003): 181-207.

Schettino, A. and E. Turco. Breakup of Pangaea and plate kinematics of the central Atlantic and Atlas regions. Geophys. Jour. Intern. 178 (2009): 1078-1097.

Shchipansky, A., and S. Bogdanova. The Sarmatian Crustal Segment: Precambrian Correlation between the Voronezh Massif and the Ukrainian Shield across the Dniepr-Donets Aulacogen. Tectonophysics 268 (1996): 109-25.

Torcq, F., J. Besse, D. Vaslet, J. Marcoux, L. E. Ricou, M. Halawani, and M. Basahel. Paleomagnetic results from Saudi Arabia and the Permo-Triassic Pangaea configuration. Earth Planet. Sci. Lett. 148 (1997): 553-67.

Torsvik, T.H. Super-IAPD. Computer software. Geodynamics - Software & Databases. Vers. 2000. Web. 30 Jan. 2010. <http://www.geodynamics.no/software.htm>.

Torsvik, T.H. and L.R.M. Cocks. Earth geography from 400 to 250 million years: a palaeomagnetic, faunal and facies review. Jour. Geol. Soc. 161 (2004): 555-572.

Torsvik, T.H., R.D. Müller, R. Van der Voo, B. Steinberger, and C. Gaina. Global Plate Motion Frames: Toward a unified model. Rev. Geophys. 46 (2008): RG3004.

Torsvik, T.H., and R. Van der Voo. Refining Gondwana and Pangaea Paleogeography: estimates of Phanerozoic non-dipole (octupole) fields. Geophys. Jour. Intern. 151 (2002): 771-94.

Vai, G.B. Development of the paleogeography of Pangaea from Late Carboniferous to Early Permian. Paleogeogr. Paleoclim., Paleoecol. 196 (2003): 125-155.

Van der Voo, R., and T.H. Torsvik. Evidence for late Paleozoic and Mesozoic non-dipole fields provides an explanation for the Pangaea reconstruction problems. Earth Planet. Sci. Lett. 187 (2001): 71-81.

Van der Voo, R., and T.H. Torsvik. The Quality of European Permo-Triassic Paleopoles and its impact on Pangea Reconstructions, in: Timescales of the paleomagnetic field, J.E.T. Channell, D.V. Kent, W. Lowrie and J. G. Meert, Editors, AGU Geophysical Monograph, 145 (2004): 29-42.

Vizán, H., and M.A. Zele. Analysis of a Permo-Triassic polarity transition in different absolute reconstructions of Pangaea, considering a model with features of the present Earth magnetic field. Annals Geophys. 50.2 (2007): 191-202.

Wegener, A., Die Entstehung der Kontinente , Peterm. Geogr. Mitt. 58I (1912): 185–195, 253–256, 305–309.

White, C. Permian elements in the Dunkard flora. Geological Society of America Bulletin. 16 (1904).

Zijderveld, J.D.A. A.C. demagnetization of rocks: analysis of results. In: Methods in paleomagnetism , D.W. Collinson, K.M. Creer and S.K. Runcorn (eds). Elsevier (1967): 254-286.

Table and Figure Captions.

Table 1. Site-mean magnetization directions and statistical parameters

Site	**n**	**z**	**GPS lat (N)**	**GPS long (E)**	**D°**	**I°**	**k**	**α95°**
Andesites and one baked contact (site K104-K110)								
K001-K009	9	9	47°48.104'N	38°01.020'E	226.5	-61.3	186.4	3.8
K010-K016	7	6	47°32.154'N	37°47.915'E	221.1	-58.6	104.9	6.6
K017-K023	7	7	47°31.749'N	37°44.960'E	57.1	69.2	111.4	5.7
K031-K037	7	7	47°39.730'N	37°46.548'E	60.5	60.3	172.3	4.6
K038-K044	6	6	47°43.659'N	37°47.571'E	55.6	51.7	717.6	2.5
K045-K051#	7	4	47°36.234'N	37°57.461'E	*172.8*	*76.6*	*339.5*	*5.0*
K076-K084	8	8	47°13.179'N	37°05.966'E	267.8	-63.1	136.4	4.8
K085-K091	6	5	47°13.215'N	37°05.957'E	253.2	-64.0	519.9	3.6
K092-K093*	2	2	47°13.215'N	37°05.985'E	*235.1*	*-59.8*	*82.5*	*27.8*
K111-K117	7	7	47°39.627'N	37°57.358'E	236.7	-71.7	93.4	7.0
K178-K184**,#	7	0	47°18.251'N	37°47.097'E				
M1200	7	6	47° 31.737'N	37° 44.968'E	56.5	65.9	92.5	7.0
M1208	7	6	47° 39.763'N	37° 46.407'E	63.3	66.8	127.0	6.0
M1223	7	7	47° 13.265'N	37° 05.852'E	262.1	-64.5	118.2	5.6
K104-K110	6	6	47°39.655'N	37°57.265'E	224.6	-67.1	240.4	3.9
Site	**n**	**z**	**GPS lat (N)**	**GPS long (E)**	**D°**	**I°**	**k**	**α95**
Trachytes								
K052-K058*	4	3	47°37.408'N	37°52.321'E	*324.4*	*70.0*	*11.3*	*38.5*
K059-K065	6	4	47°37.388'N	37°52.252'E	199.3	-36.0	56.1	12.4
K097-K103	7	7	47°39.655'N	37°57.265'E	213.2	-38.6	144.2	5.0
K118-K124*	6	6	47°39.732'N	37°58.105'E	*288.4*	*3.6*	*5.4*	*28.7*
K125-K130*	4	3	47°39.732'N	37°58.105'E	*22.8*	*68.7*	*12.1*	*37.1*
K131-K137*	7	3	47°39.690'N	37°57.948'E	*212.4*	*-32.7*	*5.5*	*58.8*
K138-K142	5	4	47°19.169'N	37°45.434'E	203.2	-7.2	73.0	10.8
K143-K149	7	4	47°19.218'N	37°45.610'E	204.7	3.1	205.8	6.4
K150-K156	7	7	47°19.216'N	37°45.680'E	218.0	-12.0	100.9	6.0
K157-K163	7	5	47°19.176'N	37°45.711'E	215.0	-4.4	18.3	18.4
K164-K171	8	7	47°19.031'N	37°45.915'E	219.5	-7.5	36.2	10.2
K172-K178	7	6	47°18.828'N	37°46.401'E	217.3	-6.8	36.7	11.2
K185-K191*	7	4	47°18.225'N	37°46.984'E	*213.9*	*5.9*	*12.7*	*26.9*
K192-K198	7	6	47°18.490'N	37°50.582'E	196.7	-21.1	140.3	5.7
K199-K204	5	5	47°18.597'N	37°50.555'E	194.9	-17.4	93.4	8.0
K205-K211	6	6	47°18.691'N	37°50.698'E	188.6	-16.2	159.5	5.3
K212-K218**	7	0	47°39.315'N	37°58.353'E				
M1171	7	6	47° 18.992'N	37° 49.132'E	217.6	-40.7	109.4	6.4

M1178	7	6	47° 20.848’N	37° 52.367’E	197.6	-14.4	87.3	7.2
M1185	7	6	47° 20.531’N	37° 51.677’E	217.0	-26.5	140.9	5.7
M1192	7	7	47° 20.55’N	37° 51.748’E	206.8	-37.1	101.7	6.0
D1-HT	10	7	47° 20'N	37° 52'E	205.8	-24.0	22.2	13.1
D3*	7	4	47° 20'N	37° 51'E	*195.4*	*-18.0*	*15.8*	*23.8*
D9*	7	5	47° 37.383’N	37° 52.250’E	*201.9*	*-37.5*	*10.8*	*24.4*
D10-5d1	7	6	47° 39.683’N	37° 57.950’E	180.4	-26.2	14.9	18.2
D13	6	5	47° 18.680’N	37° 50.645’E	193.6	-26.2	540.7	3.3
D14-HTC	6	6	47° 39.303’N	37° 58.297’E	203.5	-43.1	205.1	4.7
D11&D12	5	4	47° 19.210’N	37° 45.713’E	218.6	-18.4	275.0	5.6

N = Total number of samples collected per site
n = Number of samples demagnetized
z = Number of samples used for calculation/analysis
declination correction of 7.2° has been applied to all results
* = sites with k lower than 10, or alpha-95 higher than 20 ° have been excluded and entered in italics
** = sites where the magnetization was eliminated for >95% at <200°C, entered in italics
# = sites with mean directions that are very aberrant, entered in italics
H = hematite, M = magnetite
Site K024-K030 had mislabeled samples so it was not measured.

Table 1. Site-mean directions obtained from thermal demagnetization plot results: D° = declination angle, I° = inclination angle, k = precision parameter k, α_{95}° = radius of 95% confidence around mean direction, n = Number of samples demagnetized; z = Number of samples used for calculation/analysis; *= sites with k lower than 10, or alpha-95 higher than 20° have been excluded and entered in italics; **= sites where the magnetization was eliminated for >95% at <200°C, entered in italics; # = sites with mean directions that are very aberrant, entered in italics. A declination correction of 7.2° has been applied to all results.

Table 2. Mean Directions, paleopoles

Mineralogy	D°	I°	k	α_{95}°	N	VGP Lat (°)	VGP Long (°)	VGP dp	VGP dm
Andesite (reversed)	241.4	-65.4	75.1	7	7				
Andesite (normal)	58.4	62.8	128.7	6.8	5				
Andesite (combined)	240.1	-64.4	96	4.5	12	50 N	106.4 E	5.8	7.2
Trachyte	205.6	-21.4	23	7	20	47.5 N	179.2	3.9	7.4

Overall mean directions of the andesite and trachyte collections and paleopoles with the semi-major and sem-minor axes of the oval of 95% confidence (dp, dm). Other explanations as in Table 1.

Table 3. Results of the 40Ar-39Ar age dating of hornblendes from one trachyte sample (M1171) and eight andesite samples. For M1171, two steps are not enough to calculate an isochron. For M1199, the steps do not overlap, so an acceptable isochron cannot be calculated. The steps for M1207 and M1216 yielded several ages ranging over half a billion years and could not be used.

Sample	Mineral	J-value	Steps used (Temp)	cum39Ar (%)	Spectrum age	1s (w.o. J)	1s (w. J)	Isochron age	1s (w.o. J)	1s (w. J)	Sums	40Ar/36Ar	1s
M1171	Hornblende	0.005881	6 to 7 987-1055C	82.7	**282.6** Weighted mean	**0.05**	**2.6**						
M1199	Hornblende	0.005880	6 to 11 986-1117C	89.7	**204.2** Weighted mean	**0.03**	**1.6**						
M1207	Hornblende	0.005873											
M1208	Hornblende	0.005834	8 to 11 1025-1102C	83.8	209.0 Plateau age	0.05	2.0	**209.2**	**1.0**	**2.2**	1.36	293.6	5.7
M1213	Hornblende	0.005878	10 to 13 1085-1263C	94.8	208.2 Plateau age	0.08	1.9	**209.3**	**0.1**	**2.0**	0.02	283.3	7.4
M1215	Hornblende	0.005860	9 to 12 1032-1153C	89.7	209.4 Plateau age	0.06	2.0	**210.7**	**1.2**	**2.3**	2.43	285.4	10.5
M1216	Hornblende	0.005875											
M1226	Hornblende	0.005884	10 to 13 1079-1211	58.3	214.9 Plateau age	0.02	2.0	**215.7**	**0.4**	**2.0**	0.37	278.6	17
M1234	Hornblende	0.005857	7 to 10 920-1073C	79.2	209.2 Plateau age	0.05	2.0	**208.9**	**0.8**	**2.1**	1.99	296.5	3.6

A conservative 1% uncertainty is assumed for all J values
Preferred ages in bold (isochron age preferred)

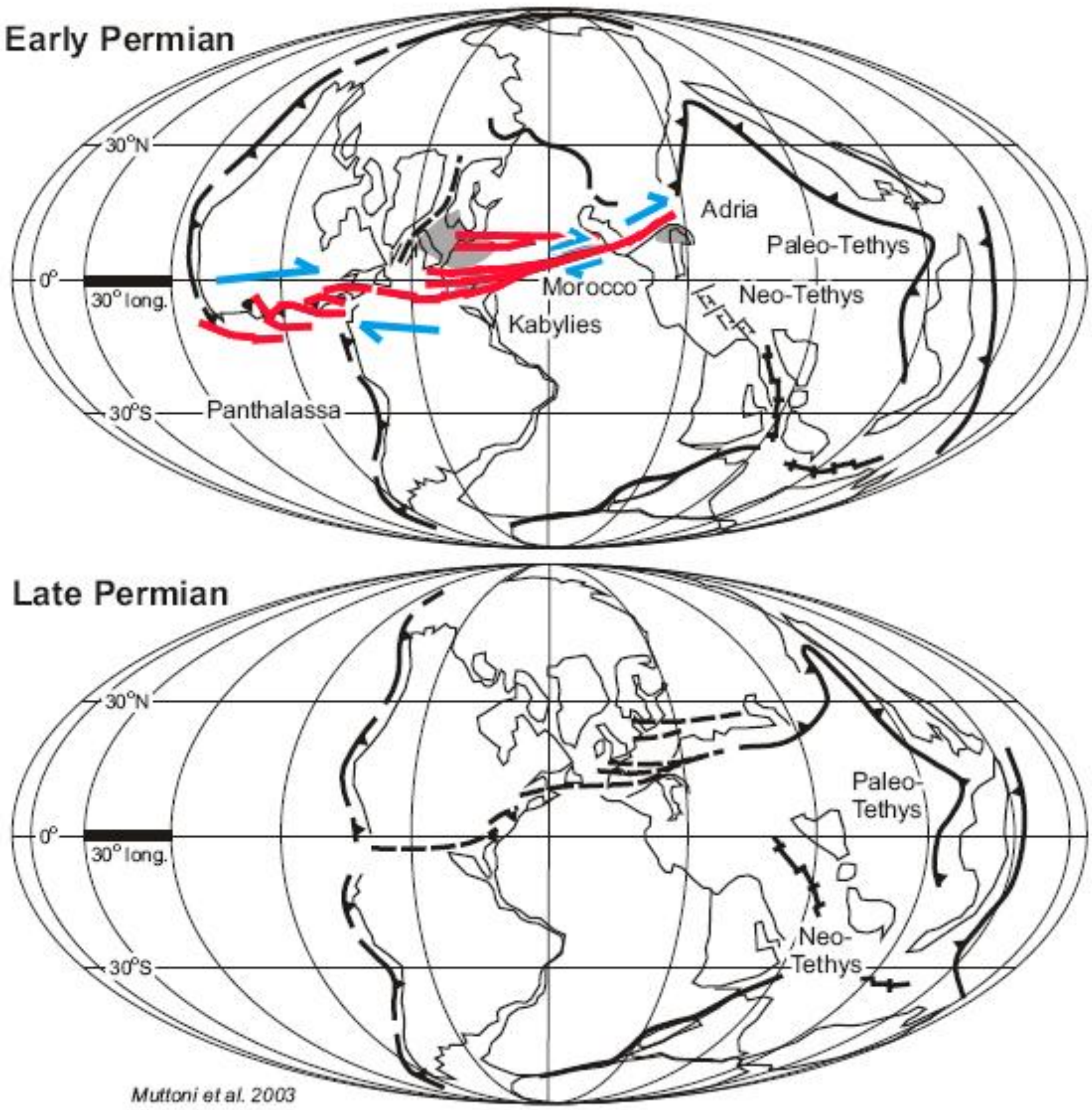

Figure 1. Pangaea B (top), changing into Pangea A (bottom) along an WSW-ENE dextral megashear of some 3500 km length between Laurussia and Gondwana (from Muttoni et al., (2003).

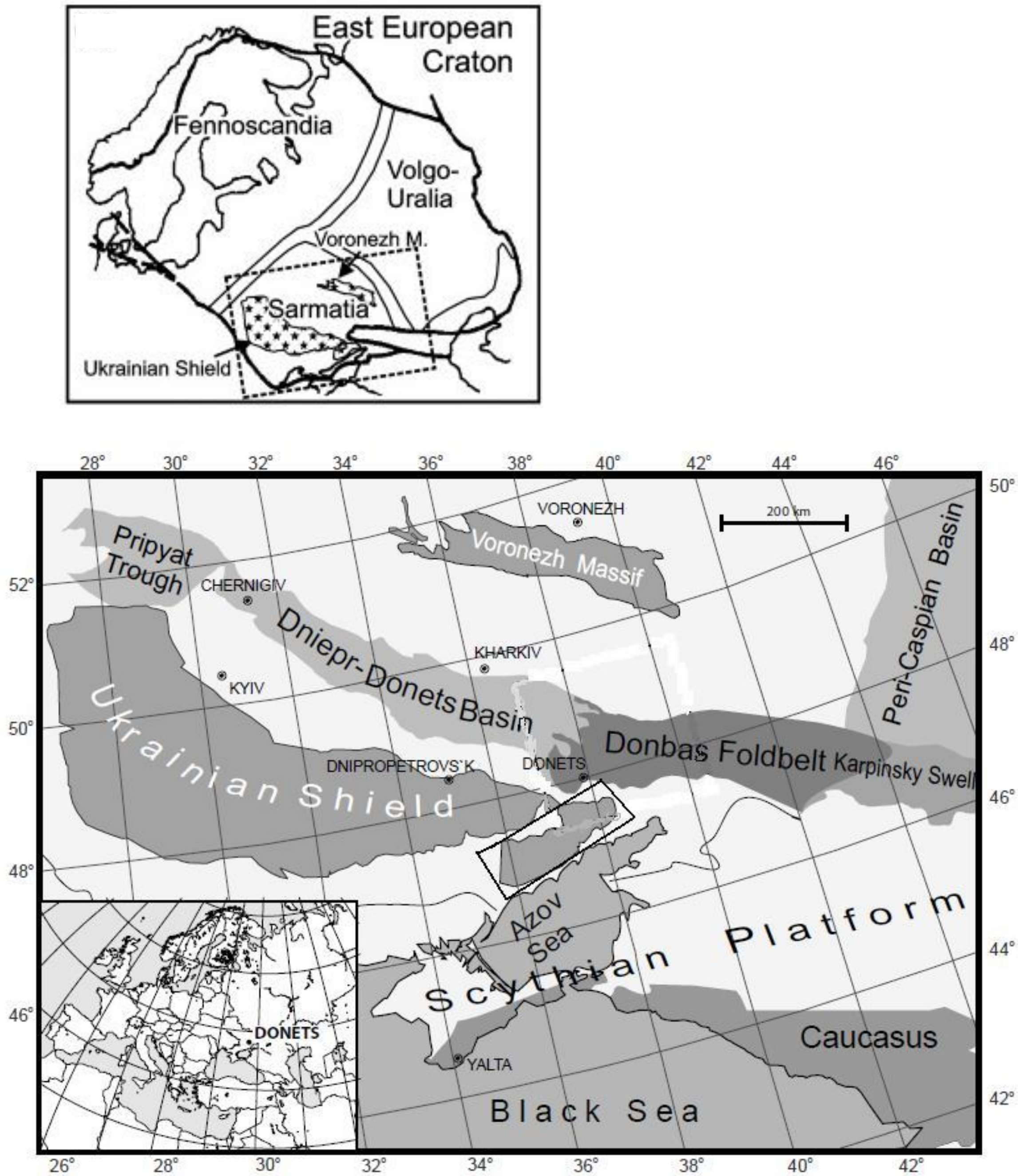

Figure 2. Geographical map of the East European Craton (Danišík, 2008) and geologic map of its Ukrainian Shield (Meijers, 2010). The Ukrainian shield, the sampling area, is in the southwest half of Sarmatia and has been circled with an oval.

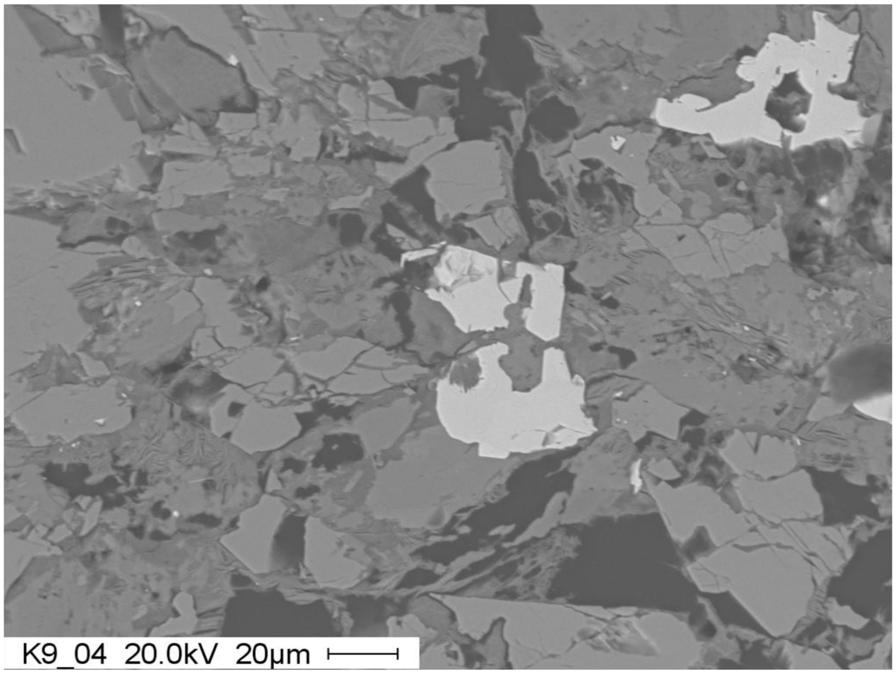

Figure 3. An SEM scan of a representative andesite thin section with a titanomagnetite containing cations totaling 23 weight % titanium and 76 weight % iron for the bright grain on the bottom of the center. No shrinkage cracks in the analysis show that there has been no alteration (maghemitization). There are no lamellae present, which further demonstrate that there was no alteration (exsolution/oxidation).

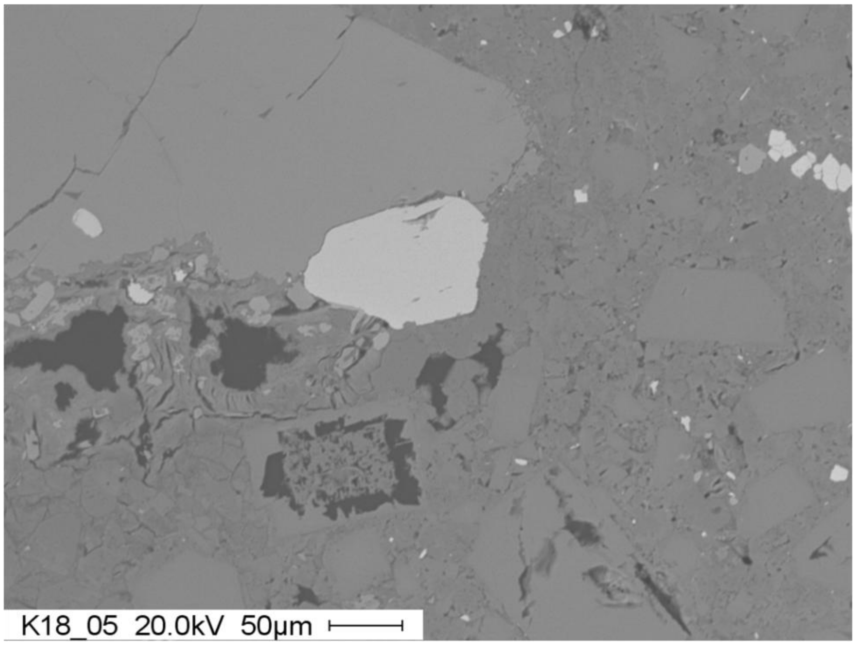

Figure 4. An SEM scan of a representative andesite grain with 43 weight % titanium and 57 weight % iron. No shrinkage cracks in the analysis show that there has been no alteration. The bright grain in the center, which was analyzed, is representative of the potential magnetic carriers (Fe-oxides).

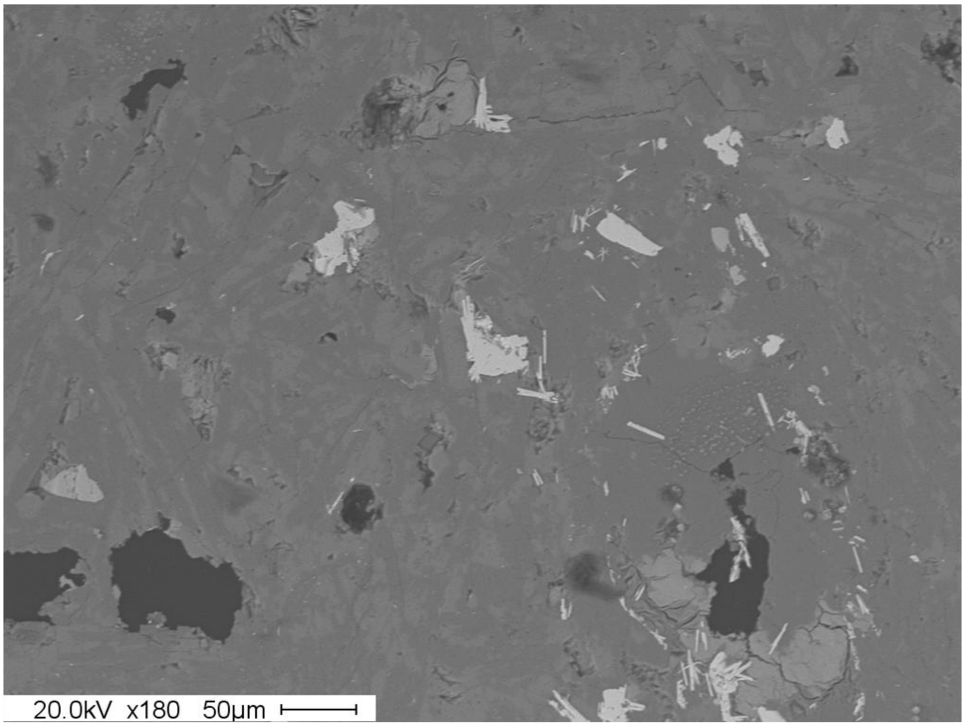

Figure 5. An SEM scan of a grain in a representative trachyte sample with 4 weight % titanium and 96 weight % iron. No shrinkage cracks in the analysis show that there has been no alteration.

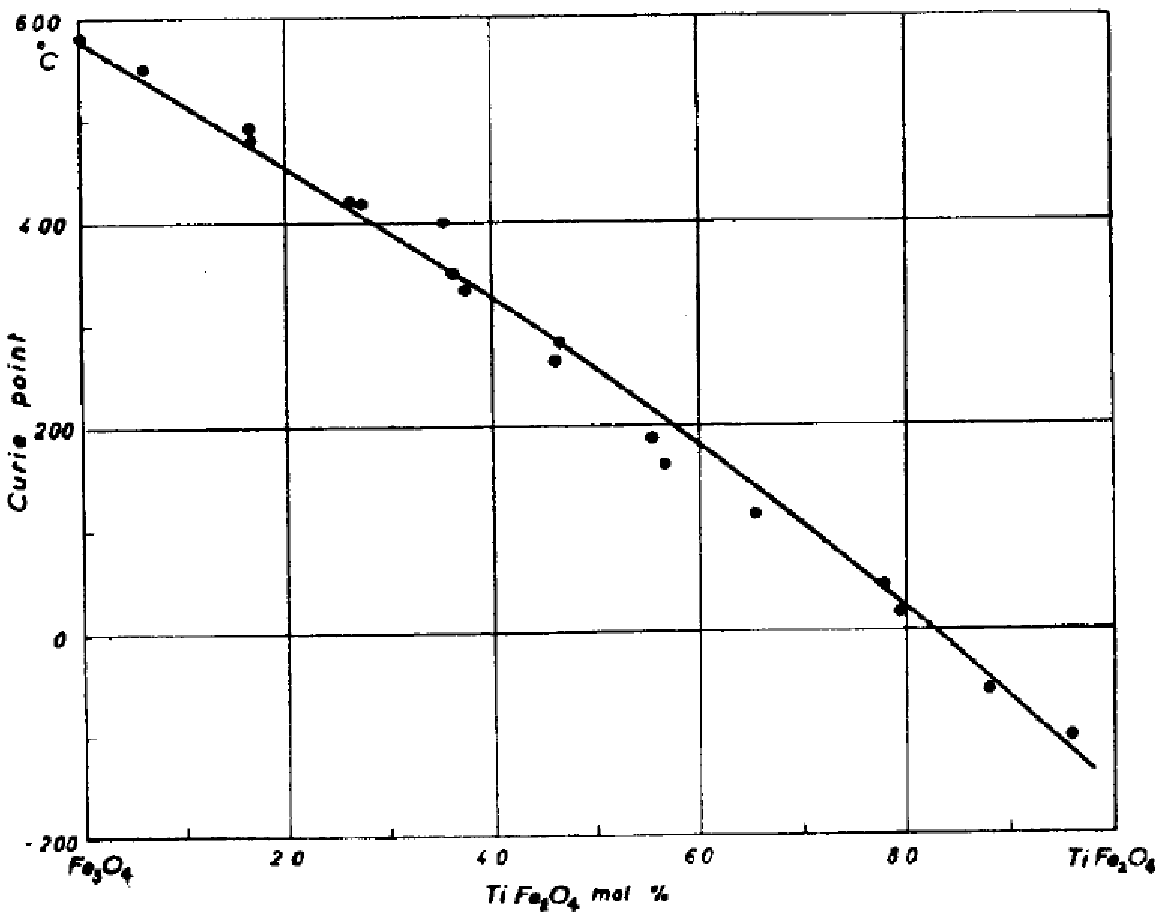

Figure 6. From Akimoto 1957. A diagram showing how substituting titanium into the magnetite lowers the Curie temperature. The 43% titanium and 57 % Fe corresponds to an unblocking temperature of about 300°C. This would not have any effect on the sample as those grains with such a high titanium content would be instantaneously remagnetized by the VRM. Moreover, the grain that was analyzed is not representative of the whole sample.

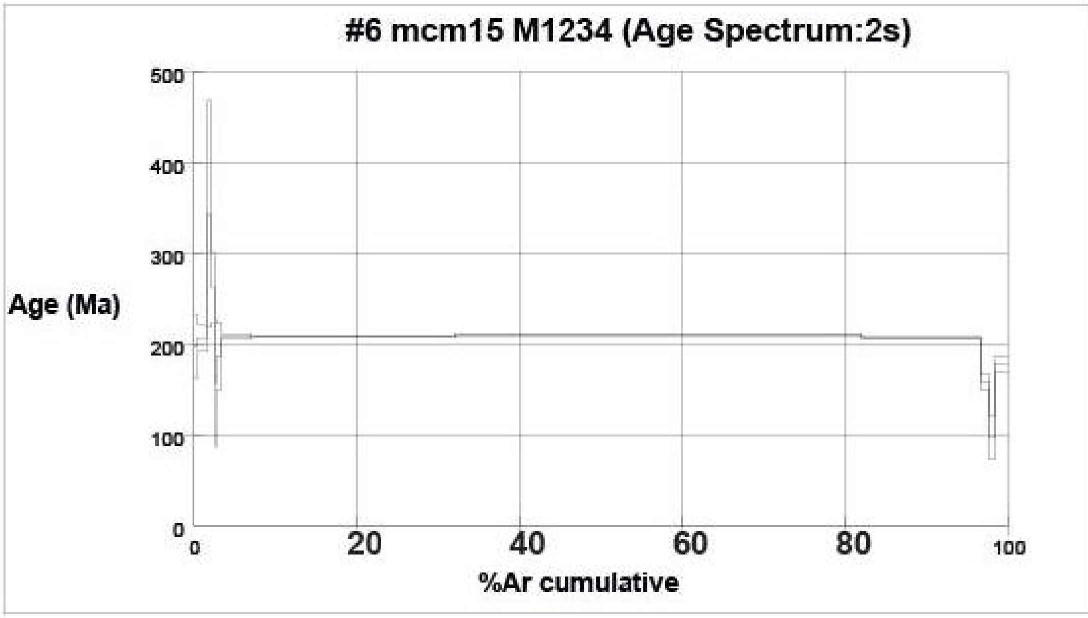

Figure 7. The plateau age of 209.2 ± 2.0 Ma (1 sigma, with and without J uncertainty) comes from steps 7-10 at 920-1073°C where 79.2 % of the argon is released in these three stages.

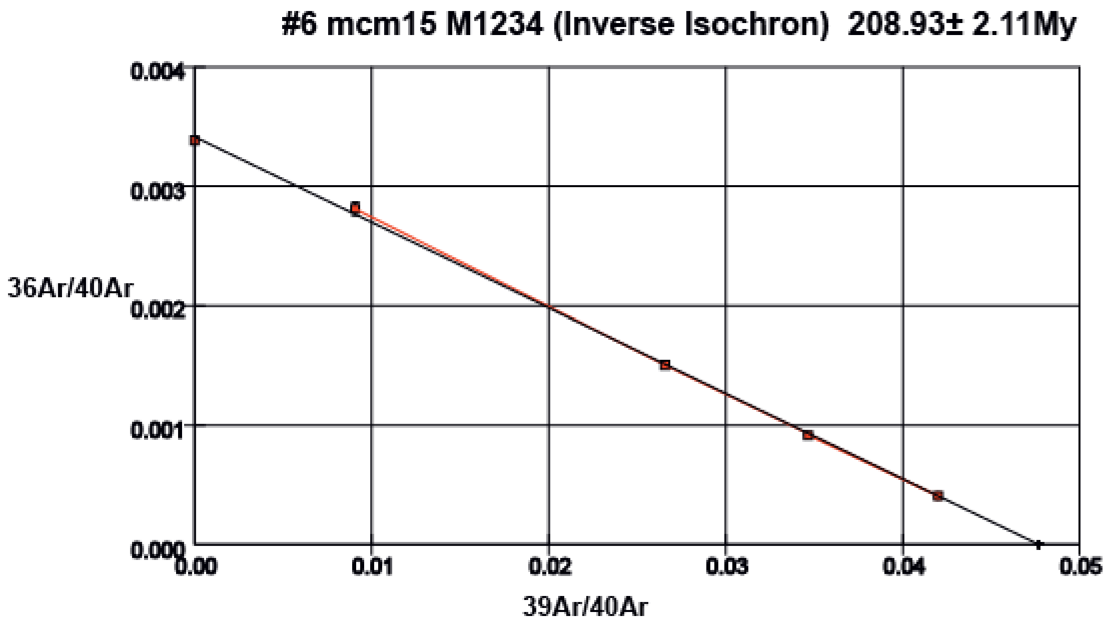

Figure 8. The isochron has an age of 208.9 ± 2.1 Ma (with and without one sigma of uncertainty). The sum of squares at 1.99 means it is a statistically good isochron. There is a 40/36 intercept of 296.5 ± 3.6 Ma (overlapping atmospheric level at 95 % confidence level).

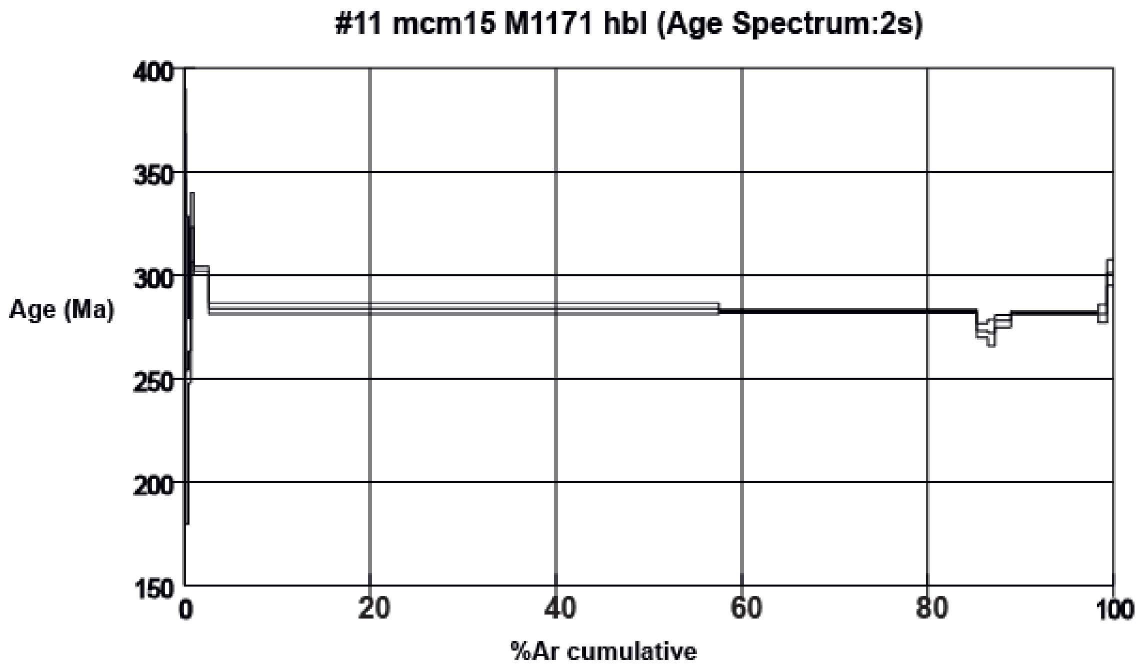

Figure 9. Six step isochron of the trachyte for an age of 280-285.2 Ma. The weighted mean average for steps 6 and 7 (987-1055°C) has 82.7 % of accumulated released. This correlates to an age of 282.6 ± (0.5 Ma) 2.6 Ma (one sigma, without and with J uncertainty). Although the J uncertainty is high—about one percent—the steps are stable and the paleomagnetism of the region clearly points to a Permian direction.

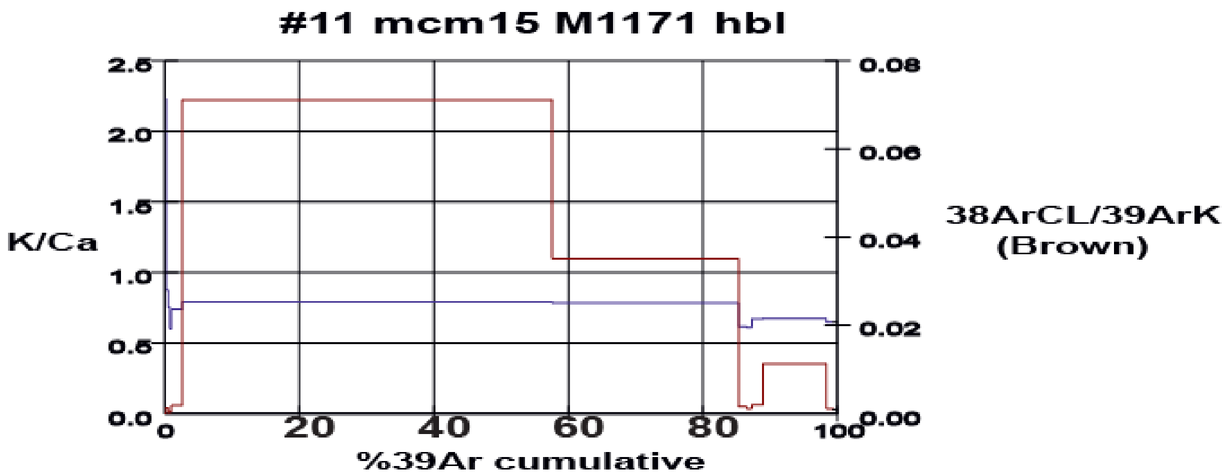

Figure 10. This graph of the K/Ca and 38 ArCl/39ArK content has a drop between steps 8-10, which correlates to the drop in the same steps of the isochron.

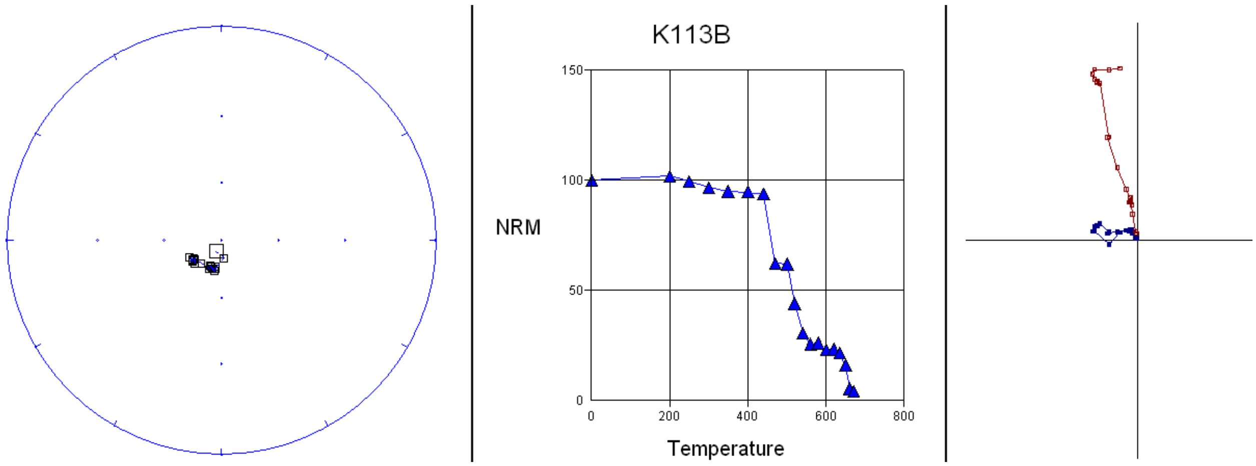

Figure 11. In this case a very small overprint can be seen from 0-250°C and was clearly not an ancient component. The rest of the sample has two components—a LTC and a HTC—the former's temperature steps are from 250-580°C and the latter's from 580-670°C. As a result, the LTC's carrier is mostly magnetite while the HTC's carrier is mostly hematite. The LTC and HTC components in this sample are steeply southwesterly and up; they have similar directions and the HTC was arbitrarily chosen.

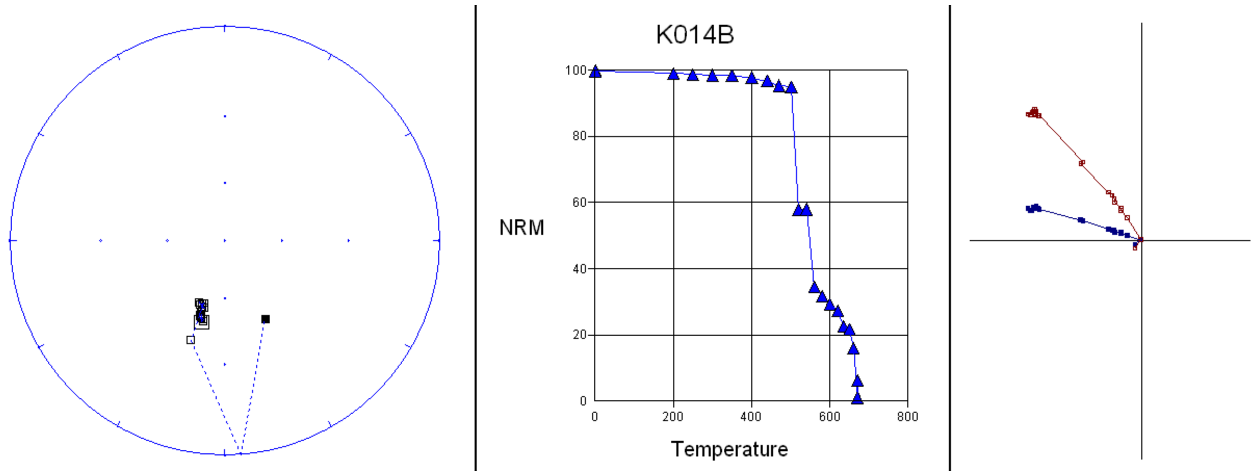

Figure 12. This plot of sample K014B (andesite) represents the easily interpretable samples from the dataset. Note that the decay is almost univectorial but actually consists of two components. One component exists from 0-560°C and the other from 580-670°C. The first component's carrier is magnetite because unblocking in that temperature interval represents magnetite while the second one is hematite because it decays by 670°C. This sample and other samples from this site have little to no alteration and both components lie steeply up in the southwest direction. Either the higher or lower temperature component could have been used because they have similar declinations and inclinations but the higher one was arbitrarily chosen. Many of the andesites behaved in this fashion.

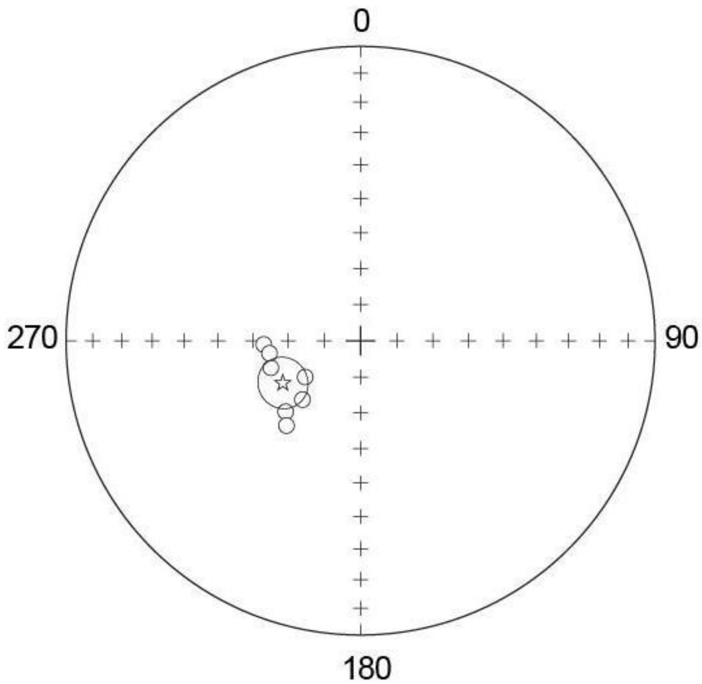

Figure 13. A plot of all the andesite reversed polarity site means. Mean declination = 241.4, mean inclination = -65.4, K = 75.1, a95 = 7.0, N = 7.

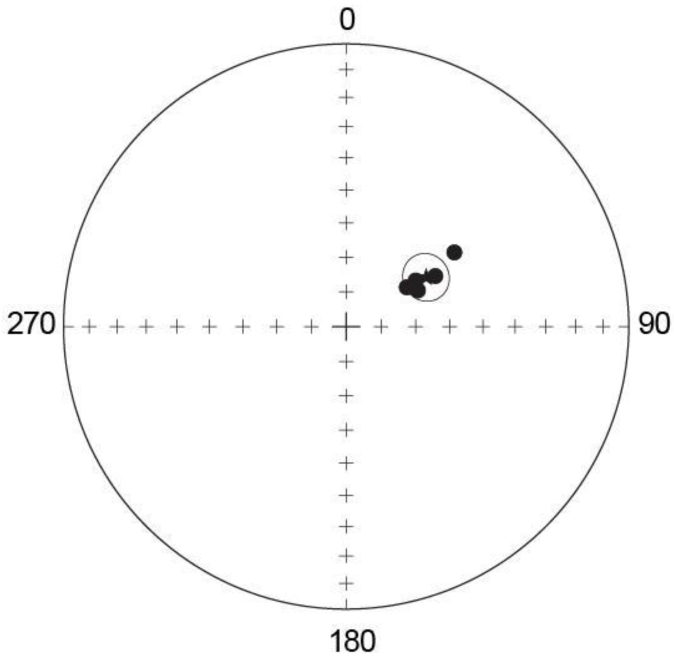

Figure 14. A plot of all the andesite normal polarity site means. Mean declination = 58.4, mean inclination = 62.8, K = 128.7, a95 = 6.8, N = 5.

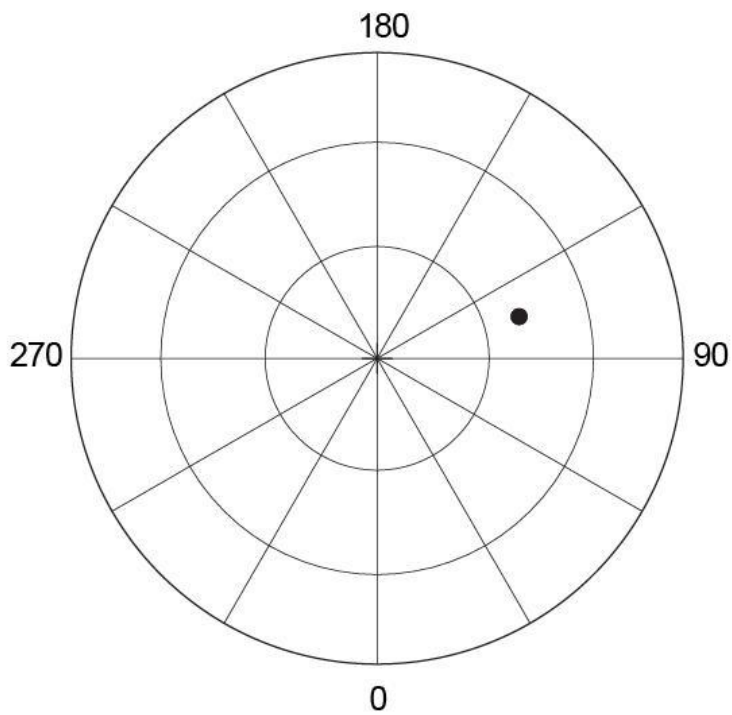

Figure 15. VGP for the andesites. 50° N, 106.4° E, dp = 5.8°, dm = 7.2°

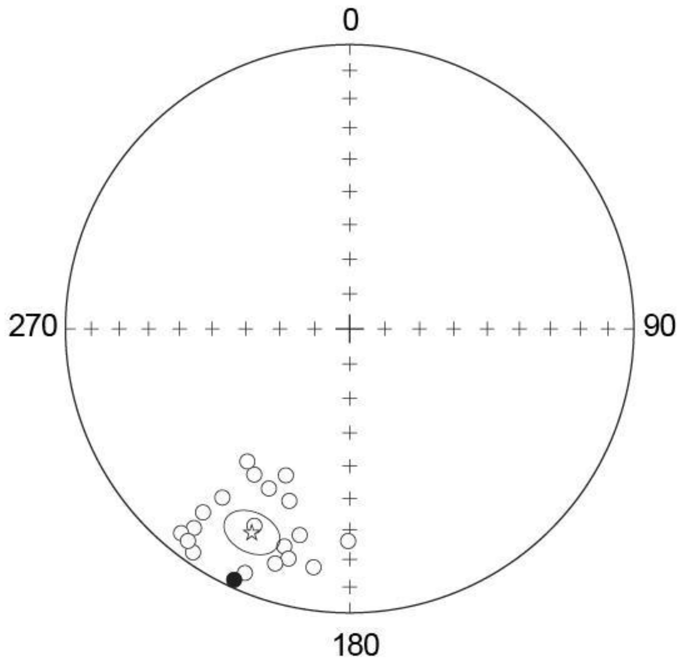

Figure 16. A plot of all the trachyte site means. Mean declination = 205.6, mean inclination = -21.4, K = 23.0, a95 = 7.0, N=20.

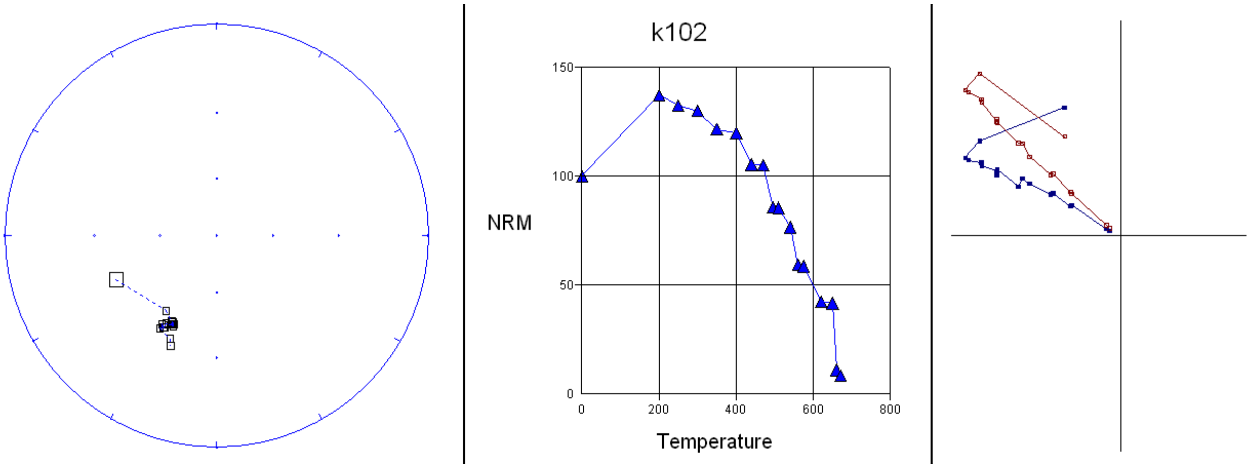

Figure 17. The plot of sample K102 (trachyte) represents the samples that required more complicated analysis than other plots. There are two components in this sample and the lower component from 0-200°C represents secondary magnetization because it points approximately in the same direction as the present day magnetic field of the Ukrainian shield (northerly and down). There are two other components from 300-580°C and 580-670°C which represent the characteristic magnetization and which is south-southwesterly and intermediately up. Most trachyte samples were similarly affected by a present day magnetic field overprint. Both the LTC (likely carried by magnetite below 580°C) and HTC (hematite) components have the same directions within error.

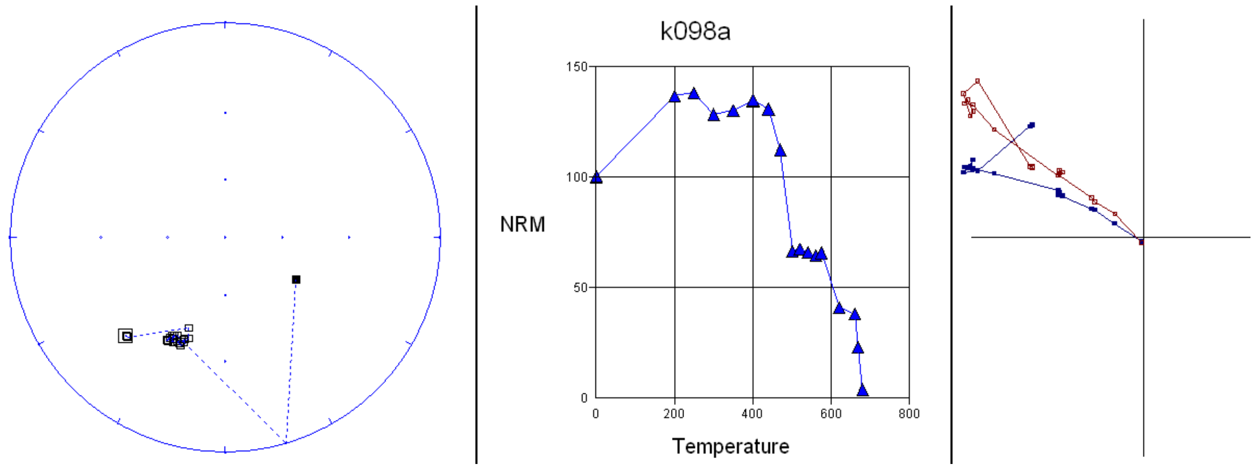

Figure 18. K098A (trachyte) shows a complex magnetic history in that it has three components. There is an overprint from the present day magnetic field removed below 200°C, and two upward and southwesterly components that are the magnetizations acquired during formation. The first southwesterly component (LTC) is removed from 200-575°C and the HTC one from 620-680°C. Therefore, the 200-575°C component is mostly magnetite while the HTC is hematite. The HTC and LTC have similar directions.

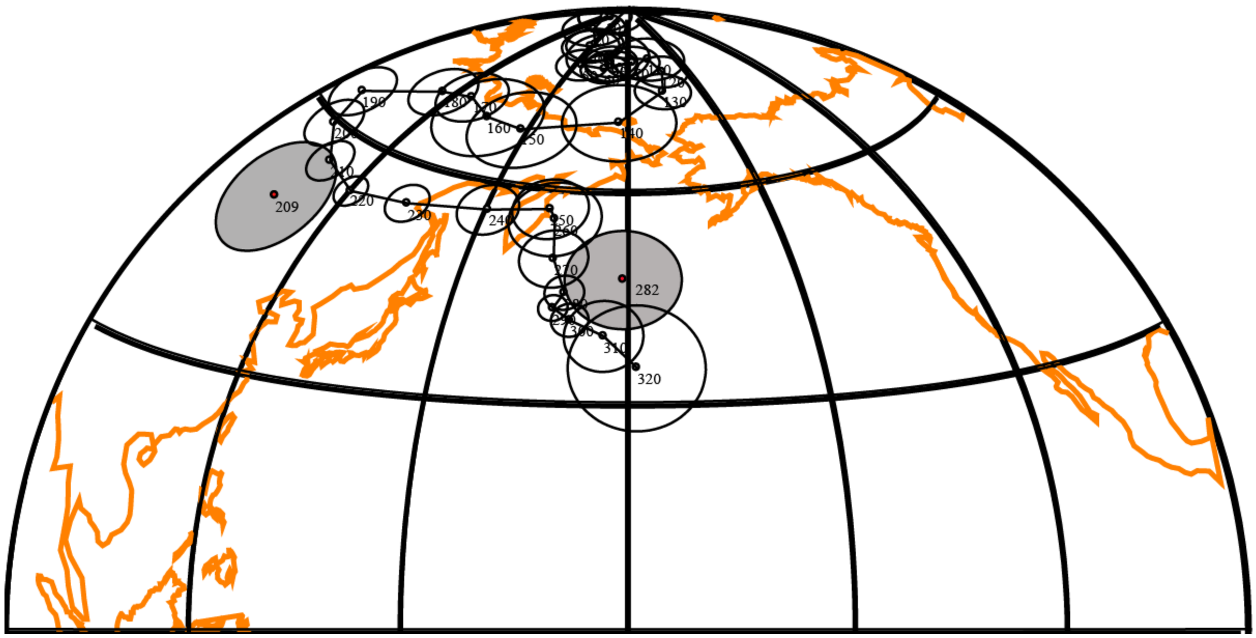

Figure 19. APWP from Torsvik (2008). The VGPs are plotted against the APWP for Baltica.

Figure 20. Paleogeographical map of data fitted for Pangaea.

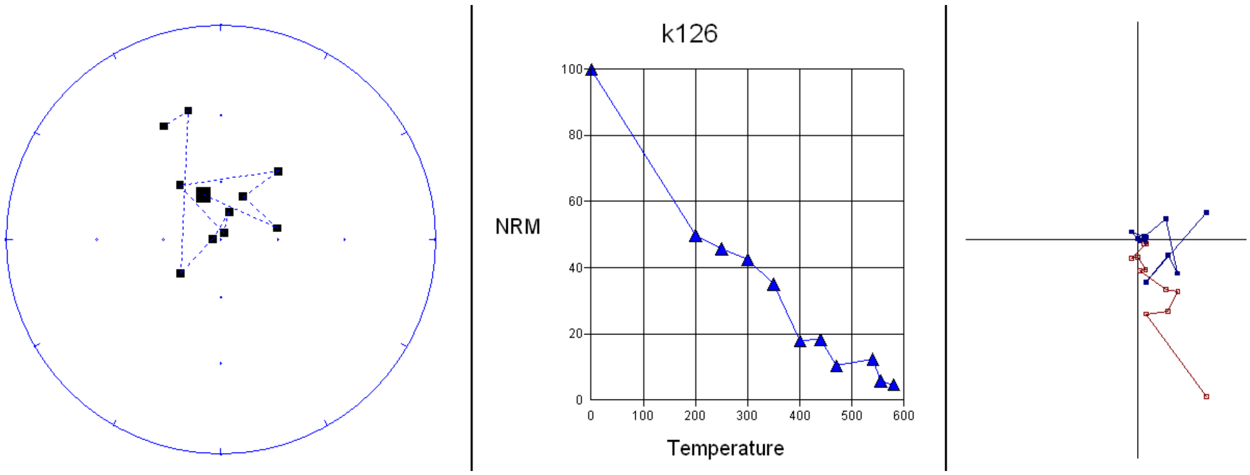

Figure 21. This plot of sample K126 (trachyte) represents a demagnetization that could not be interpreted in terms of Permian geomagnetic field directions. The magnetization of the sample starts dropping immediately at heating and decays steadily until 580°C at which point there is less than five percent magnetization left. The carrier of the magnetization is likely magnetite. There were several trajectories that varied widely in direction. The higher temperature trajectory in this sample did not correspond to the other higher temperature trajectory in other samples from the trachyte dikes. In fact, this whole site had oddly behaving trajectories and was not used for the study.